

Photospheric abundances of the rapidly-rotating A-type star Altair

Yoichi Takeda

11-2 Enomachi, Naka-ku, Hiroshima-city, 730-0851, Japan.

Contributing authors: ytakeda@js2.so-net.ne.jp;

Abstract

Altair is an A-type star known to have an appreciably oblate shape owing to its very fast rotation ($\sim 300 \text{ km s}^{-1}$). Despite of numerous publications on this star, its chemical abundances have been scarcely investigated so far, presumably because of the practical difficulty that spectral lines are considerably broadened by rapid rotation and badly blended with each other. Motivated by this situation, a spectroscopic analysis was conducted to study the photospheric abundances of Altair by using the synthetic spectrum-fitting technique, in order to clarify whether or not any chemical peculiarities exist. The microturbulent velocity was determined to be $2.9 (\pm 0.9) \text{ km s}^{-1}$ by requiring that the metallicity does not show any systematic region-dependence. Then, the abundances of 17 elements (C, N, O, Mg, Al, Si, S, Ca, Sc, Ti, Cr, Mn, Fe, Ni, Zn, Sr, Ba) were derived, where the non-LTE effect was taken into consideration as much as possible. The results revealed considerable region-by-region dispersion (several tenths dex or even more), reflecting the difficulty of reliable abundance determination for such a very rapid rotator. Nevertheless, the differential mean abundances relative to the Sun turned out to fall within $-0.5 \lesssim [X/H] \lesssim +0.3$ for all elements without any dependence upon the atomic number. Accordingly, we may conclude that (1) no appreciable anomalies of chemical abundance patterns exist in the atmosphere of Altair, (2) but its global metallicity is likely to be slightly subsolar (~ -0.2 dex on the average).

Keywords: stars: abundances – stars: atmospheres – stars: early-type – stars: individual (Altair) – stars: rotation

1 Introduction

Altair (= α Aql = HR 7557 = HD 187642 = HIP 97649) is an A-type main-sequence star (spectral type: A7 V), which is easily recognizable as a first-magnitude star ($V = +0.76$ mag) near to the Milky Way in the sky of summer night.

It is notable that this star is spectroscopically known to rotate very rapidly ($v_e \sin i \sim 200\text{--}250 \text{ km s}^{-1}$, where v_e is the equatorial rotational velocity and i is the inclination angle of rotational axis). Although this is not uncommon in A-type stars, the remarkable feature of Altair is that the

effect of rapid rotation (e.g., flattening effect or gravitational darkening) is directly measurable by interferometric observations thanks to its proximity from us (distance of only 5.14 pc according to the *Hipparcos* parallax). Actually, the parameters relevant to such a flattened rotator (e.g., effective temperature T_{eff} and radius R at the pole and equator, etc.) as well as v_e and i have been separately determined interferometrically, as summarized in Table 1. As such, the physical condition over the surface of Altair is rather well understood nowadays.

Table 1 Altair’s parameters determined by interferometric observations.

| Literature (1) | M (2) | $T_{\text{eff,p}}$ (3) | $T_{\text{eff,e}}$ (4) | R_p (5) | R_e (6) | v_e (7) | i (8) | $v_e \sin i$ (9) | β (10) | Remark (11) |
|----------------------------------|------------|---------------------------|---------------------------|--------------|--------------|--------------|------------|---------------------|-----------------|----------------|
| van Belle et al. (2001) | | 7680 | | 1.887 | | | | 210 | | |
| Ohishi et al. (2004) | | 7750 | | | | | | | | |
| Domiciano de Souza et al. (2005) | 1.8 | 8500 | 6509 | 1.711 | 2.117 | 277 | 55 | 227 | 0.25 | |
| Peterson et al. (2006) | | 8740 | 6890 | 1.636 | 1.988 | 273 | 64 | 245 | 0.25 | |
| Monnier et al. (2007) | 1.791 | 8450 | 6860 | 1.634 | 2.029 | 285 | 57.2 | 240 | 0.19 | adopted here |
| Hadjara et al. (2014) | 1.791 | 8912 | 7372 | 1.639 | 2.000 | 269 | 57.3 | 226 | 0.19 | |
| Bouchaud et al. (2020) | 1.86 | 8621 | 6780 | 1.565 | 2.008 | 313 | 50.65 | 242 | 0.185 | |
| input/output of SEDINT | 1.8 | 8450 | 6884 | 1.63 | 2.02 | 285 | 57 | 239 | 0.19 | |

(1) Reference. (2) Mass (in unit of the solar mass M_\odot). (3) Polar effective temperature (in K). (4) Equatorial effective temperature (in K), (5) Polar radius (in unit of the solar radius R_\odot). (6) Equatorial radius (in R_\odot). (7) Rotational velocity at the equator (in km s^{-1}). (8) Inclination angle of the rotational axis (in degree). (9) Projected rotational velocity (in km s^{-1}). (10) Gravitational darkening parameter ($T_{\text{eff}} \propto g^\beta$). (11) Specific remark. At the last row, the input parameters (M , $T_{\text{eff,p}}$, R_p , v_e , i , and β ; taken from Monnier et al.) along with the output results ($T_{\text{eff,e}}$ and R_e) of the SEDINT program are also presented.

In contrast, regarding the surface abundances of Altair, an important topic in connection with chemical peculiarities often seen in A-type stars, little is known unfortunately, since trials of elemental abundance determinations for this star have been scarce. To the author’s knowledge, two spectroscopic studies have worked upon Altair’s chemical abundances of various elements (though the global metallicity was reported in some other work; cf. Table 2). That is, Erspamer and North (2003) included Altair in their abundance studies for 140 A–F stars. In addition, Altair was also included in Luck (2017)’s recent spectroscopic study for parameters and abundances of 1002 stars in the local region, though his project was essentially focused on late-type stars (F, G, and K dwarfs and giants).

However, their consequences are not consistent with each other. For example, regarding the microturbulence (v_t) and Fe abundance ($[\text{Fe}/\text{H}]$), Erspamer and North (2003) derived 2.0 km s^{-1} and -0.24 dex , while appreciably larger values of 5.7 km s^{-1} and $+0.48 \text{ dex}$ resulted from Luck (2017)’s analysis. Besides, abundance patterns are apparently different. Luck (2017)’s results show considerable overabundances ($[\text{X}/\text{H}] \gtrsim 0.5$; some are even $1 \lesssim [\text{X}/\text{H}] \lesssim 2$) in heavier elements (Ti, V, Cr, Mn, Fe, Co, Ni, Y, Zr, Ce, Nd, Eu, except for Ba which is underabundant), but Ca and Sc are inversely underabundant ($[\text{X}/\text{H}] \lesssim -0.5$), interestingly suggesting characteristic peculiarities seen in A-type metallic-line (Am) stars. On the other hand, such Am-like trends are not observed in

the $[\text{X}/\text{H}]$ values derived by Erspamer and North (2003), which tend to be within $-0.3 \lesssim [\text{X}/\text{H}] \lesssim +0.3$ for many elements, excepting that overabundances of Na, Sc, Co, La, Nd by $\sim +0.5\text{--}0.9 \text{ dex}$ while a large underabundance of Sr by $\sim -2 \text{ dex}$.

Presumably, such a paucity of chemical abundance studies and diversified results for Altair are due to the fact that reliable abundance determinations are very difficult for such a conspicuously rapid rotator ($v_e \sin i \sim 200\text{--}250 \text{ km s}^{-1}$), in which spectral lines are considerably broadened and blurred out, causing serious blending with each other. Actually, chemical abundances of A-type stars with $v_e \sin i \gtrsim 200 \text{ km s}^{-1}$ seem to have been rarely investigated so far. though trials for moderately fast rotators ($100 < v_e \sin i < 200 \text{ km s}^{-1}$) turned out somehow feasible if carefully done (e.g., Lemke 1993).

In this investigation, we try to challenge this hard task of establishing the photospheric elemental abundances of Altair. The aim is to clarify whether or not this very rapidly-rotating A-type star in the solar neighborhood shows any chemical peculiarities.

It has been generally believed that the key parameter for the emergence of Am-like chemical peculiarities (CP) in A stars (which may possibly be related to element diffusion process requiring the stability of the atmosphere/envelope) is the rotational velocity, in the sense that the anomaly emerges for slowly rotating stars while it is suppressed for the case of rapid rotation. However, the critical rotational velocity demarcating CP and

non-CP groups is not yet well understood. While [Abt and Morrell \(1995\)](#) stated that A5–F0 stars with $v_e \sin i > 120 \text{ km s}^{-1}$ are normal stars (cf. their fig. 6), some chemical anomaly in C and Ba might still persist up to $v_e \sin i \lesssim 180 \text{ km s}^{-1}$ as seen from [Lemke \(1993\)](#)’s fig. 3. Therefore, it is interesting to examine whether or not any Am-like abundance peculiarities (deficiencies of light elements such as C, N, and O as well as Sc or Ca; overabundances of heavy elements such as s-process ones) are observed in Altair, an intrinsically very rapid rotator with v_e as large as $\sim 300 \text{ km s}^{-1}$.

Alternatively, there is another group of chemically peculiar stars (so-called λ Boo stars) which show deficiencies in refractory Fe group elements (presumably caused by dust–gas separation mechanism) while volatile elements (such as CNO) remain almost normal (e.g., [Venn and Lambert 1990](#)). Since most stars of this group are rapid rotators, it may be possible that Altair shows this kind of anomaly, since K -band excess indicating circumstellar dust emission is observed ([Nuñez et al. 2017](#)). Accordingly, abundances of volatile and refractory elements should be compared each other in order to see if there is any difference between these.

Methodologically, since application of spectrum-synthesis technique is mandatory for the present case, we extensively employ the spectrum-fitting code developed by [Takeda \(1995\)](#). This flux-based method (using only arbitrarily-scaled spectrum) is advantageous, because it does not require any precise continuum normalization in advance, which is difficult especially for rapid rotators.

2 Atmospheric model parameters

As usual, we employ the conventional plane-parallel model atmosphere for abundance determination, which is characterized by T_{eff} (effective temperature) and $\log g$ (logarithmic surface gravity). However, since (i) these parameters are significantly latitude-dependent [$T_{\text{eff}}(\theta)$, $\log g(\theta)$] over the stellar surface and (ii) how these surface inhomogeneities affect the observed stellar flux depends upon the aspect angle of rotation (i) in

the present case, we have to find “adequately averaged” $\langle T_{\text{eff}} \rangle$ and $\langle \log g \rangle$ of Altair. Here, we invoke a theoretical rotating star model in order to calculate the intensity distribution (I) at any point of the stellar disk. Then, $\langle T_{\text{eff}} \rangle$ and $\langle \log g \rangle$ may be derived by averaging the local T_{eff} and $\log g$ over the visible disk while weighting them with the corresponding brightness. This is the approach which was adopted also by [Takeda \(2023a\)](#).

For this purpose, the program SEDINT developed by [Takeda et al. \(2008\)](#) was used, which simulates the spectral energy distribution (SED) of a rotating star based on the Roche model. That is, SEDINT calculates the local specific intensity directed toward the observer $I_\lambda(\xi, \eta)$ at each disk point (ξ, η) projected on the sky, from which the theoretical flux observed at the earth (F_λ) is derived by integration as

$$F_\lambda \equiv \iint_{\text{disk}} I_\lambda(\xi, \eta) \, d\xi d\eta / d^2 \quad (1)$$

where d is the distance to Altair (5.14 pc).

The input parameters of SEDINT are M (stellar mass), $T_{\text{eff,p}}$ (effective temperature at the pole), R_p (polar radius), v_e (equatorial rotational velocity), β (gravitational darkening parameter), and i (inclination angle). As to the local model atmospheres, solar-metallicity models were employed. Regarding these six parameters, we decided to adopt the values derived by [Monnier et al. \(2007\)](#) (cf. the last row in Table 1), because the resulting F_λ satisfactorily matches the observed SED (f_λ) by this choice. This is demonstrated in Fig. 1a (blue line), where the results corresponding to [Hadjara et al. \(2014\)](#)’s parameters ($T_{\text{eff,p}}$ higher by ~ 400 – 500 K) are also shown for comparison (green line).

Then, we may define $\langle T_{\text{eff}} \rangle$ (mean T_{eff} averaged over the disk) and $\langle \log g \rangle$ (mean $\log g$ averaged over the disk) as

$$\langle T_{\text{eff}} \rangle \equiv \frac{\iint_{\text{disk}} T_{\text{eff}}(\xi, \eta) I_{5000}(\xi, \eta) \, d\xi d\eta}{\iint_{\text{disk}} I_{5000}(\xi, \eta) \, d\xi d\eta} \quad (2)$$

and

$$\langle \log g \rangle \equiv \frac{\iint_{\text{disk}} \log g(\xi, \eta) I_{5000}(\xi, \eta) \, d\xi d\eta}{\iint_{\text{disk}} I_{5000}(\xi, \eta) \, d\xi d\eta}, \quad (3)$$

where I_{5000} is the specific intensity at 5000 \AA .

The values of $\langle T_{\text{eff}} \rangle$ and $\langle \log g \rangle$ resulting from Eqs. (2) and (3) are 7663 K and 4.04. Accordingly, we adopt $T_{\text{eff}} = 7660$ K (rounded value) and $\log g = 4.04$ as the standard parameters of Altair, and the corresponding Kurucz (1993)'s ATLAS9 solar-metallicity model is used for abundance determination. The flux calculated with this model by using the ATLAS9 program agrees well with the observed SED as shown in Fig. 1b. Such established T_{eff} and $\log g$ are also compared with various literature values in Table 2.

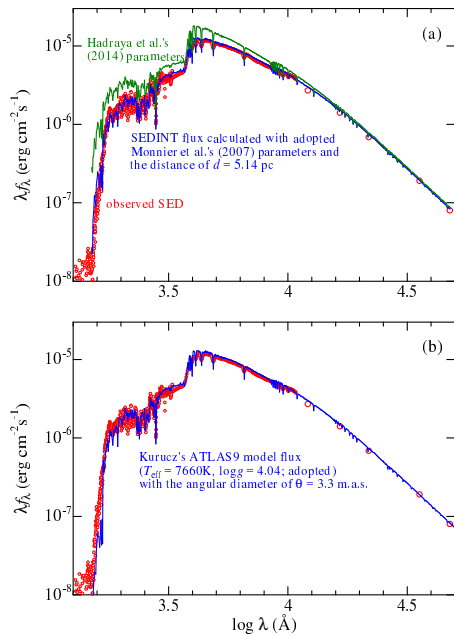


Fig. 1 Theoretically calculated spectral energy distributions (SED) (depicted in lines) are compared with the observed SED of Altair (red symbols). The observational data were taken from the archive data of International Ultraviolet Explorer (SWP48485LL+LWP15801LL) in the UV region, Alekseeva et al. (1996) in the visible region, and Bouchet et al. (1991) with Cohen et al. (1992)'s calibration in the infrared region (*JHKLM* band). (a) Theoretical SED was calculated from the gravity-darkened rotating star model by using the SEDINT program (Takeda et al. 2008) by using Monnier et al. (2007)'s parameters we adopted (blue lines). In addition, the result with Hadjara et al. (2014)'s parameters (not adopted) is also depicted in green lines for reference. (b) Theoretical SED (blue lines) is the flux calculated from Kurucz (1993)'s ATLAS9 solar-metallicity model corresponding to $(T_{\text{eff}}, \log g) = (7660 \text{ K}, 4.04)$ adopted in this study.

3 Method and data for the analysis

3.1 Spectrum fitting method

In this investigation, we extensively employ the stellar spectrum analysis tool MPFIT (Takeda 1995), which was developed based on Kurucz (1993)'s ATLAS9/WIDTH9 program and has a function of establishing the spectrum-related parameters (elemental abundances, microturbulence, macrobroadening parameters, radial velocity shift, etc.) by automatically searching for the best-fit solutions without any necessity of precisely placing the continuum level in advance.

In applying this method to the spectra of Altair, where shallow and heavily blended line features distribute over wide wavelength ranges (several tens of Å), it is essential to introduce not only the scale-controlling constant (C) but also the tilt-adjustment parameter (α) in comparing the observed flux (f_{λ} ; in arbitrary scale) with the theoretical flux (F_{λ}) in order to accomplish a satisfactory fit. That is, the right-hand side of equation (1) in Takeda (1995) is redefined as $\sum \{\log f_{\lambda} - \log F_{\lambda} - C - \alpha(\lambda - \lambda_{\min})/(\lambda_{\max} - \lambda_{\min})\}/N$, and the best values of C and α are iteratively established, where λ_{\max} and λ_{\min} are the maximum and minimum wavelength of the relevant region.

In the present case, the parameters to be varied to achieve the best fit are (i) the abundances of selected N elements (A_1, A_2, \dots, A_N ; cf. Table 3), (ii) the projected rotational velocity ($v_e \sin i$), and (iii) the wavelength shift ($\Delta\lambda_r$). The abundances of all other elements remain unchanged at the solar abundances (i.e., model atmosphere values), and the microturbulence (v_t) is fixed (which is determined in Sect. 4.1). The assumption of LTE (Local Thermodynamic Equilibrium) is postulated at this stage of spectrum fitting analysis.

3.2 Atomic line data

Regarding the data (wavelength, excitation potential, gf value, damping parameters) of spectral lines in the relevant wavelength regions (3900–9300 Å), we exclusively consulted Vienna Atomic Line Database¹ (Ryabchikova et al. 2015). Because the data were downloaded about 10 years

¹<https://vald.astro.uu.se/>

Table 2 Conventional atmospheric parameters of Altair adopted in past publications.

| Literature (1) | T_{eff} (2) | $\log g$ (3) | v_t (4) | [Fe/H] (5) | Remark (6) |
|------------------------------|-------------------------|-----------------|--------------|---------------|---|
| Sokolov (1995) | 8040 | | | | Use of Balmer continuum slope |
| Di Benedetto (1998) | 7568 | | | | Use of $V - K$ color |
| Erspamer and North (2003) | 7550 | 4.13 | 2.0 | -0.24 | Chemical abundance analysis |
| Gray et al. (2003) | 7800 | 3.76 | 2.0 | +0.02* | Fitting with synthetic spectrum |
| Allende Prieto et al. (2004) | 7646 | 4.23 | | | Photometric T_{eff} , $\log g$ from isochrones |
| Zorec and Royer (2012) | 7727 | | | | Use of $wby\beta$ color |
| Luck (2017) | 7377 | 3.95 | 5.7 | +0.48 | Chemical abundance analysis |
| Borisov et al. (2023) | 7485 | 3.72 | | -0.08* | Fitting with synthetic spectrum grid |
| This study | 7660 | 4.04 | 2.9 | -0.12 | |

(1) Reference. (2) Effective temperature (in K). (3) Logarithmic surface gravity (in c.g.s unit). (4) Microturbulent velocity dispersion (in km s^{-1}). (5) Fe abundance relative to the Sun (in dex). (6) Specific remark. At the last row, the parameters derived/adopted in this study are also given for comparison.

*This value corresponds to [M/H] (metallicity; i.e., logarithmic scale factor common to all elements applied to solar compositions).

ago (2016 July) and not the latest, some modifications were further applied. (1) As the gf values of a number of neutral carbon lines turned out to be too large in the old data, all the data of C I lines were replaced by those newly downloaded in 2026 January. (2) Since the gf values of two Si I lines at 6353.3597 and 6353.5188 Å were found to be unreasonably large, these two lines were excluded.

3.3 Observational data

As to the observed spectra of Altair, the data published by Allende Prieto et al. (2004) were basically employed in this study, which are the data resulting from the project ‘‘Spectroscopic Survey of Stars in the Solar Neighborhood’’ (abbreviated as S⁴N).² These spectra (with a resolving power of $R \sim 50000$) have sufficiently high signal-to-noise ratio of several hundred and cover the wavelength range of 3630–10440 Å.

In addition, the spectra of the UVES Paranal Observatory Project (UVES-POP)³ (Bagnulo et al. 2003) were also used for several specific regions, because S⁴N spectra have some spike-like feature (λ 4465–4495 Å region) or telluric lines are less severe for the case of the UVES-POP spectra ($\lambda > 9000$ Å region).

When necessary, telluric lines were removed by hand-drawing the upper envelope for five conspicuously contaminated spectral regions, as depicted in Fig. 2.

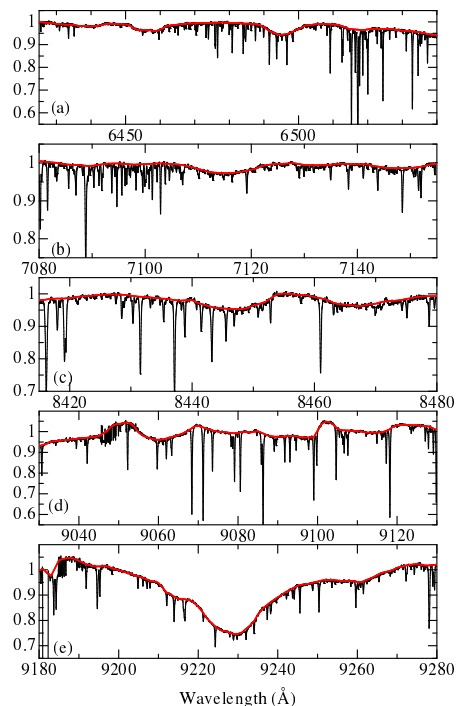


Fig. 2 How the telluric lines were eliminated by hand-drawing the upper envelope (red) of the real spectrum (black) is shown in five regions: (a) 6425–6540 Å region, (b) 7080–7155 Å region, (c) 8415–8480 Å region, (d) 9030–9130 Å region, and (e) 9180–9280 Å region.

²<https://hebe.as.utexas.edu/s4n/>

³<https://www.eso.org/sci/observing/tools/uvespop.html>

4 Determination of elemental abundances

4.1 Microturbulence

Before deriving chemical abundances, we have to evaluate the microturbulent velocity, an important parameter for abundance determination. Usually, this parameter is determined by requiring that the abundances derived from various lines (Fe lines in most cases) do not show any systematic strength-dependent trend.

Since heavily blended spectra are concerned here and accuracy or difficulty in deriving the abundance for a specific element (e.g., Fe) differs from case to case, we follow a somewhat modified approach while assuming that elemental abundances are controlled by a single scaling parameter ($[M/H]$; metallicity) as $A_{*,i} = A_{\odot,i} + [M/H]$ for all elements i (such as done by Gray et al. 2003), which is not a bad approximation for the present case of Altair (as we will see in Sect. 5.1). Then, the abundance parameter to be varied is only $[M/H]$.

In order for a successful determination of v_t , it is necessary to derive $[M/H]$ from wavelength regions containing strong lines (quite sensitive to changing v_t) as well as from those with weaker lines (only weakly v_t -dependent). Since lines are generally strong and numerous at shorter wavelengths (e.g., violet region) while they get weaker and fewer at longer wavelengths (e.g., green-yellow region), we selected 56 spectral regions (each being 30 Å-wide), where their central wavelengths are changed from 3900 Å to 5000 Å with a step of 20 Å (i.e., overlapping of 5 Å with each other). The spectrum-fitting technique was then applied to each of the 56 regions to derive $[M/H]$ while changing v_t from 0.5 km s⁻¹ to 5.0 km s⁻¹ with a step of 0.5 km s⁻¹.

Although not all trials were successful (e.g., iterative solutions were not converged after all or the behavior of $[M/H]$ in response to changing v_t was anomalous), reasonable results were finally obtained for 40 regions. How the theoretical spectrum fits well with the observed one in each region is shown in Fig. 3. The resulting $[M/H]$ vs. v_t relations are depicted in Fig. 4a, and the mean $\langle[M/H]\rangle$ averaged over 40 regions as well as the corresponding standard deviation σ

are plotted against v_t in Figs. 4b and 4c, respectively. Fig. 4c suggests that the microturbulence of Altair (corresponding to the minimum of σ) is $v_t = 2.9 (\pm 0.9)$ km s⁻¹, where the probable uncertainty was estimated as done in sect. 3.2 of Takeda (2022a).

4.2 Abundances derived by spectrum fitting

Now that v_t has been established, the next task is to determine the chemical abundances of various elements. Given the motivations described in Sect. 1, special attention is paid to the following elements: (i) those representing typical Am peculiarities (underabundances in C, N, O, Ca, and Sc; overabundances in heavier species such as Fe group elements as well as s-process elements like Sr or Ba). (ii) those of volatile species (C, N, O, S, and Zn) which remain near-normal in λ Boo stars in contrast to other refractory species (such as Fe group) showing deficiencies.

After preparatory simulations of theoretical line strengths over wide wavelength ranges, followed by test trials of spectrum fitting to check the feasibility, a total of 28 regions (typically several tens of Å wide) were eventually selected and confirmed to work out. These spectral regions along with the target elements (their abundances are varied to accomplish the best fit) are summarized in Table 3, which indicates that the abundances of 17 elements (C, N, O, Mg, Al, Si, S, Ca, Sc, Ti, Cr, Mn, Fe, Ni, Zn, Sr, and Ba) were determined. The theoretical spectra corresponding to the converged solutions are compared with the observed spectra in Fig. 5 for each region.

4.3 Application of non-LTE corrections

The LTE abundances derived in Sect. 4.2 should then be non-LTE corrected wherever possible. Since multiple lines are generally involved with the fitting-based abundance of any element resulting from a specific region, the non-LTE correction to be applied is evaluated as follows.

- Let us consider an element whose LTE abundance was derived to be A from the spectrum-fitting analysis in a given region.

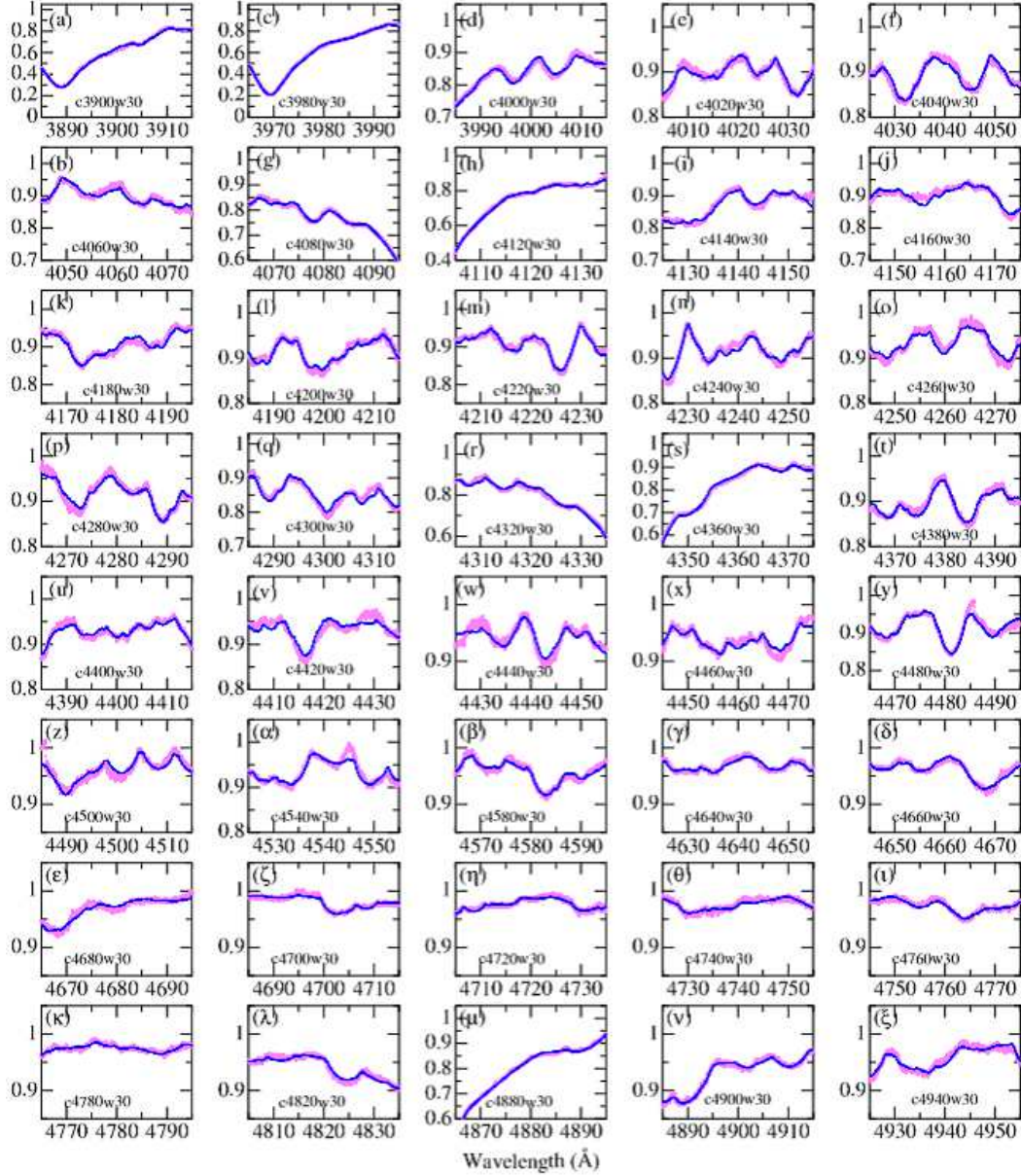


Fig. 3 Fitting of the theoretical spectrum (blue lines) with the observed spectrum (pink symbols) by adjusting $[M/H]$ at each of the 40 regions (the region code is indicated in each panel, where “c???w**” means that the center/width of the region is $??? \text{Å}/** \text{Å}$) for the purpose of v_t determination. The wavelength scale of the spectrum is adjusted to the laboratory frame, and the scale marked in the left ordinate corresponds to the theoretical residual flux ($F_\lambda^{\text{th}}/F_{\text{cont}}^{\text{th}}$)

- First, the values of η_0 ($\equiv l_0/\kappa$; line-center to continuum opacity ratio at $\tau_{5000} \sim 0.2$) are evaluated by using this A for all available lines of this element included in this region.
- Then, we select only K lines of appreciable strengths out of them, according to the criterion

of satisfying the condition $\eta_0 > 0.1$; and their theoretical equivalent widths are calculated as ($W_i, i = 1, 2, \dots, K$).

- For these K lines, the non-LTE corrections corresponding to each W_i are computed as ($\Delta_i, i = 1, 2, \dots, K$).

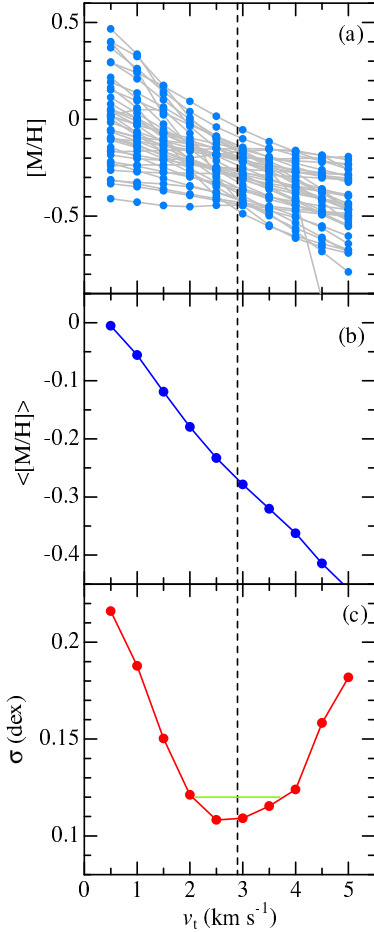


Fig. 4 (a) $[M/H]$ vs. v_t diagram constructed from the $[M/H]$ results of 40 regions derived with 10 v_t values (0.5, 1.0, 1.5, ..., 4.5, and 5.0 km s^{-1}). (b) $\langle [M/H] \rangle$ (mean $[M/H]$ averaged for all 40 regions) plotted against v_t . (c) σ (standard deviation of $[M/H]$) plotted against v_t . The green horizontal segment denotes the possible uncertainty of v_t ($\pm 0.9 \text{ km s}^{-1}$) around the minimum- σ solution (2.9 km s^{-1}), which was estimated from the fluctuation of σ based on the numerical simulation (cf. sect. 3.2 in Takeda 2022a). At each panel, the position of $v_t = 2.9 \text{ km s}^{-1}$ is indicated by the vertical dashed line.

- Now, the mean non-LTE correction ($\langle \Delta \rangle$) is defined as the weighted average of Δ_i ($\langle \Delta \rangle \equiv \sum_{i=1}^K W_i \Delta_i / \sum_{i=1}^K W_i$), from which the non-LTE abundance is finally obtained as $A + \langle \Delta \rangle$.

These non-LTE corrections were calculated for 12 elements (C, N, O, Mg, Al, Si, S, Ca, Sc, Zn, Sr, and Ba) for which the author already has experiences of non-LTE calculations (cf. Table 4), while LTE was assumed ($\langle \Delta \rangle = 0$) for the other 5 elements (Ti, Cr, Mn, Fe, and Ni). Note that the

Table 3 Selected spectrum regions and target elements.

| Region code (1) | Elements (2) |
|--------------------|------------------------|
| 39253950 | Ca, Al, Fe |
| 40604090 | Fe, Sr, Ni |
| 42004230 | Ca, Sr, Fe |
| 42354265 | Fe, Sc, Cr, Mn |
| 42954315 | Fe, Ti, Ca, Sc |
| 44654495 | Mg, Ti, Fe, Ni |
| 45404570 | Ti, Fe, Cr, Ba |
| 46604690 | Fe, Sc, Ni, Zn |
| 47104745 | Fe, Ni, Zn, Cr |
| 48004830 | Cr, Ti, Mn, Zn, Ni, Fe |
| 50155045 | Fe, Ca, Ni, Sc, Si |
| 50355070 | Fe, Ni, C, Si, Ca |
| 51605200 | Mg, Fe, Ti |
| 53605400 | Fe, C, Ti |
| 60306060 | Fe, Si, S |
| 61206150 | Ca, Ba, Fe |
| 61506180 | Ca, Si, O, Fe, Ni |
| 63406380 | Si, Ca |
| 64806510 | Fe, Ca, Ba, Ti |
| 67256765 | S, Fe |
| 71007140 | Ni, C, Fe |
| 74357475 | Fe, Cr, N |
| 77607790 | O, Fe |
| 84258460 | O, Fe, Si |
| 86758705 | Fe, N, S |
| 90509080 | C |
| 92009240 | S, Mg |
| 92409280 | Mg, O |

(1) Region code of 8 characters, where “sssseeee” indicates that the fitting analysis was done in the spectrum range from ssss Å to eeee Å. (2) Elements whose abundances were varied to accomplish the best fit, while those of other elements were fixed at the solar composition.

atomic models of Sc ($Z = 21$) and Sr ($Z = 38$) were newly constructed for the purpose of this study as described below.

- The non-LTE calculations for Sc II were carried out by using the Sc II model atom comprising 89 terms (up to $3d\ 6f\ ^1H$ at 91197 cm^{-1}) and 1402 radiative transitions, which is based on the atomic data of Kurucz and Bell (1995). Though the contribution of Sc I was neglected, the levels of Sc III were taken into account in the number conservation of total Sc atoms. The hydrogenic approximation was assumed for calculating photoionization rates. Otherwise (such as the treatment of collisional rates), the procedure described in sect. 3.1.3 of Takeda (1991) was followed.

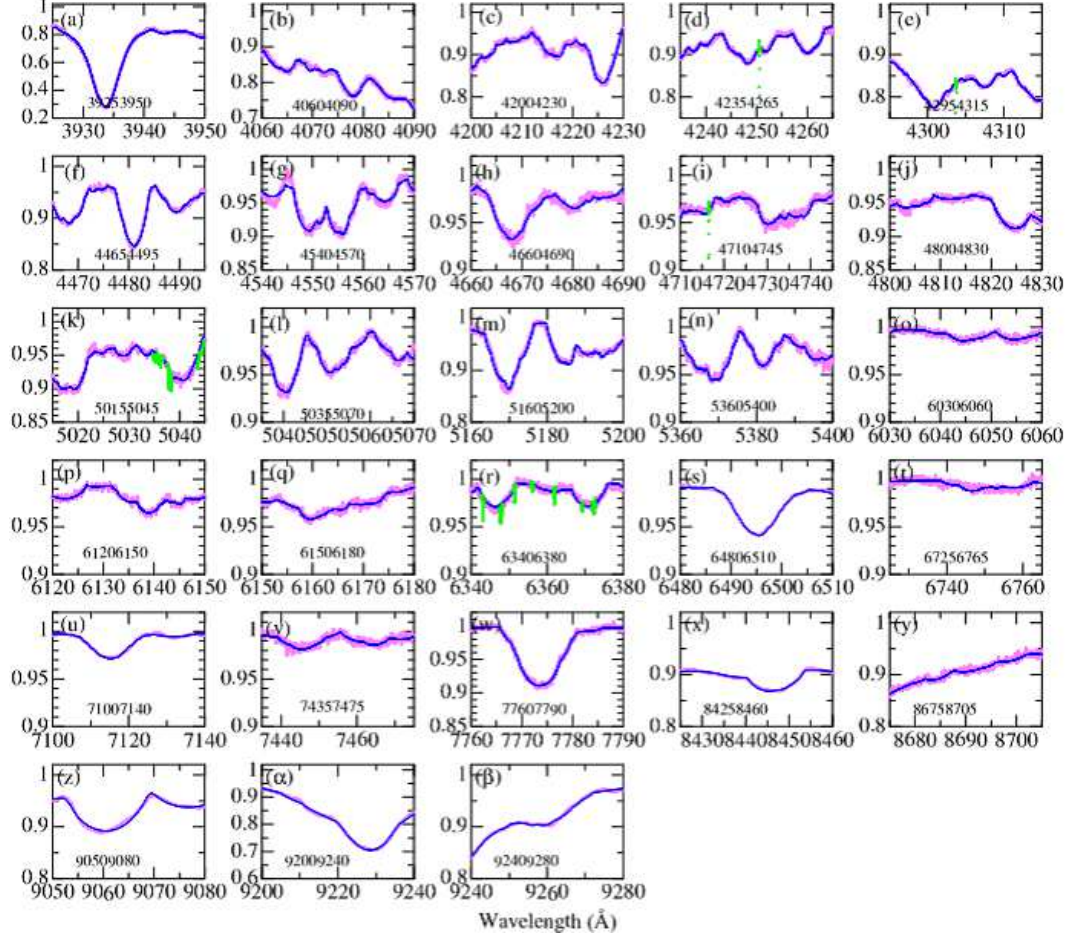


Fig. 5 Fitting of the theoretical spectrum (blue lines) with the observed spectrum (pink symbols) at each of the 28 regions (the region code is indicated in each panel) for the purpose of determining the chemical abundances of various elements. The masked portions (spectrum defect or telluric feature), which were excluded from judging the goodness of fit, are highlighted in light green. Otherwise, the same as in Fig. 3.

- Likewise, the Sr II model atom was constructed from the atomic data of Kurucz and Bell (1995), which comprises 32 terms (up to $9d^2D$ at 81249 cm^{-1}) and 54 radiative transitions. Again, the contribution of Sr I was neglected, while the levels of Sr III were taken into account in the number conservation of total Sr atoms. Regarding the photoionization cross section, the data read from fig. 1 of Mashonkina et al. (2020) were used for the lowest 3 terms ($5s^2S$, $4d^2D$, and $5p^2P^\circ$), while the hydrogenic approximation was assumed for the remaining terms. Collisional rates were calculated by following recipe in sect. 3.1.3 of Takeda (1991).

The detailed results are presented in the online supplementary materials: The non-LTE corrections (Δ_i) of individual lines as well as the resulting mean correction ($\langle\Delta\rangle$) for each element/region (along with relevant atomic line data) are given in “nltelines.dat”. Meanwhile, the region-by-region LTE/NLTE abundances and the corresponding NLTE corrections for each element are summarized in “reg.abund.dat”.

Table 4 References of non-LTE calculations.

| Elem. | Z | References |
|-------|-----|----------------------|
| (1) | (2) | (3) |
| C | 6 | Takeda (1992) |
| N | 7 | Takeda (1992) |
| O | 8 | Takeda (2003) |
| Mg | 12 | Takeda (2025) |
| Al | 13 | Takeda (2023b) |
| Si | 14 | Takeda (2022b) |
| S | 16 | Takeda et al. (2005) |
| Ca | 20 | Takeda (2020) |
| Sc | 21 | (see Sect. 4.3) |
| Zn | 30 | Takeda et al. (2005) |
| Sr | 38 | (see Sect. 4.3) |
| Ba | 56 | Takeda (2026) |

(1) Element. (2) Atomic number. (3) These papers (and the references quoted therein) may be consulted for more details about the calculations (e.g., adopted model atoms). The non-LTE calculations for these elements were done by assuming the solar abundances. This is not necessarily a bad approximation in the present case, and the resulting departure coefficients are anyhow not much sensitive to a choice of input abundances.

5 Examination of abundance results

5.1 Mean abundance and standard deviation

Based on the final abundances of 17 elements derived in Sect. 4.3, their mean values ($\langle A_*^X \rangle$) averaged over N available regions are summarized in Table 5, where the reference solar abundances (A_\odot^X), mean differential abundances relative to the Sun ($\langle [X/H] \rangle$), and the standard deviations around the mean (σ) are also presented. We consulted Anders and Grevesse (1989)’s compilation⁴ for A_\odot (except for Fe for which $A_\odot = 7.50$ was adopted), in order to maintain consistency with Kurucz (1993)’s ATLAS9 models employed in this study. The resulting mean $\langle [X/H] \rangle$ and

⁴Note that these data may be somewhat outdated especially for C, N, and O according to more recent compilations. For example, Asplund et al. (2009) derived (by taking into account the 3D effect) 8.43 (C), 7.83 (N), and 8.69 (O) for the solar photospheric abundances, which are by ~ 0.2 dex lower than by the values we adopted. For other elements, the differences between Anders and Grevesse (1989) and Asplund et al. (2009) are insignificant.

its standard deviation σ (along with individual region-by-region values of $[X/H]$) for each element are graphically depicted in Fig. 6.

An inspection of Table 5 and Fig. 6 reveals that the mean abundances averaged over regions show considerably large σ (up to ~ 0.4 – 0.5 dex or even more) for several elements. We examine below these problematic cases of $\sigma > 0.4$ (i.e., C, S, Cr, Ni, and Zn) somewhat more in detail.

5.2 Carbon

The abundance of C from the 90509080 region (9.34) is apparently an outlier compared to those (8.2–8.4) from other three regions (50355070, 53605400, 71007140). That is, the C abundance derived from the strong 9061/9062/9078 lines of multiplet 1 may still be significantly overestimated despite of their large (negative) NLTE corrections (~ -0.5 dex). If the data from this region is neglected, the mean abundance is reduced by 0.26 dex down to $\langle [C/H] \rangle = -0.27$

5.3 Sulfur

Regarding S, the abundance from the 86758705 region (7.75) is markedly larger than those (6.6–7.1) from other three regions (60306060, 67256765, 92009240). That is, the S abundance derived from the 8693–8695 triplet lines might as well be overestimated. If the data from this region is neglected, the mean abundance is reduced by 0.22 dex down to $\langle [S/H] \rangle = -0.35$

5.4 Chromium

The Cr abundances derived from 5 regions widely range over ~ 4.9 – 6.1 , among which that from the 45404570 region (4.87) is especially low. If we discard this data, the mean increases by 0.20 dex, yielding $\langle [Cr/H] \rangle = +0.17$.

5.5 Nickel

The abundances of Ni derived from 8 regions widely range over ~ 5.5 – 7.0 , among which that from the 46604690 region (7.01) is appreciably high compared to the others. If this data is rejected, the mean decreases by 0.13 dex, yielding $\langle [Ni/H] \rangle = -0.32$. Since the number of available regions is rather large ($N = 8$) in this case, the effect of excluding the outlier is comparatively less significant for this element.

5.6 Zinc

Most serious is the case of Zn abundances, because the results (5.72, 4.81, and 3.70) derived from the 46604690, 47104745, and 48004830 regions (each containing Zn I 4680, 4722, and 4810 lines) extraordinarily differ from each other, which results in a conspicuously large σ of ~ 0.8 dex. Unfortunately, we can not judge which of the three may be reliable or unreliable in this case.

5.7 Impact of excluding outlier data

We have thus evaluated how the mean abundances for C, S, Cr, and Ni vary if the data of appreciable deviations are excluded, which are on the order of ~ 0.2 dex. These changes in $\langle[X/H]\rangle$ are also indicated by red arrows in Fig. 6. As seen from this figure, the impact of these variations is not so significant as to essentially alter the global tendency of chemical abundances.

5.8 Effect of parameter changes

How the abundance results are affected by the atmospheric parameters was also examined by repeating the spectrum-fitting analysis while interchangeably varying T_{eff} by ± 200 K, $\log g$ by ± 0.2 dex, and v_t by ± 0.9 km s $^{-1}$. The amounts of variations turned out $|\delta_T| \lesssim 0.2$ dex, $|\delta_g| \lesssim 0.1$ dex, while $|\delta_v|$ is considerably diversified in the range of ~ 0.0 – 0.5 dex (~ 0.2 dex on the average) because regions containing strong saturated lines (e.g., Ba II lines) are quite v_t -sensitive. These variations are not so important as to substantially affect the qualitative trends of Fig. 6 (as was the case in Sect. 5.7),

6 Discussion

6.1 Chemical abundance trends of Altair

Given the substantial difficulty of abundance determination in such a very rapid rotator as Altair, the results are generally less reliable as compared to the case of slower rotators. Since a number of lines are intricately merged at any wavelength point under the large rotational broadening (at least over several Å wide), only a slight spectrum defect or an imperfection in the data of atomic lines would easily lead to large errors

or spurious consequences, which must be the reason for the considerable region-to-region abundance dispersion observed in several elements (cf. Sect. 5).

Yet, based on the $[X/H]$ results of 17 elements depicted in Fig. 6, we may read the following characteristics regarding the photospheric abundances of Altair.

- Fig. 6 indicates that $\langle[X/H]\rangle$ ranges within $-0.5 \lesssim \langle[X/H]\rangle \lesssim +0.3$ for all 17 elements without showing any systematic dependence upon Z , which means that any characteristic abundance patterns of CP stars (cf. Sect. 1) are absent. That is, the possibility of being an Am star (deficiency in light elements such as C, N, and O along with Ca/Sc; while overabundances of heavier elements such as Sr and Ba) is clearly excluded. Likewise, specific characteristics seen in λ Boo stars, in which volatile elements (C, N, O, S, Zn) are nearly normal whilst many other refractory species (such as Fe group ones) show appreciable deficiencies, are not observed either. Accordingly, we may state that Altair is not a chemically peculiar star but rather belongs to the group of normal stars.
- However, the metallicity of this star is not necessarily the same as that of the Sun in spite of its being in the solar neighborhood, which shows a somewhat subsolar trend. That is, the average of $\langle[X/H]\rangle$ for 17 elements given in Table 5 is -0.12 (standard deviation is 0.22), which is further lowered to -0.14 if the outlier data are excluded for C, S, Cr and Ni (see the caption of Table 5). This is almost consistent with the $[M/H]$ value ranging from ~ -0.2 to ~ -0.3 (obtained as a by-product of v_t -determination; cf. Fig. 4b). Therefore, Altair appears to have a slightly lower metallicity in comparison with the Sun, though this should not be regarded as an acquired chemical anomaly but may rather be due to fluctuations in the galactic gas at the time of star formation.

6.2 Comparison with previous studies

It has thus been shown that Altair does not belong to the group of chemically peculiar stars (occasionally observed in late A- to late B-type stars of the upper main sequence), though its metallicity

Table 5 Elemental abundance results of Altair.

| X | N | $\langle A_*^X \rangle$ | A_{\odot}^X | $\langle [X/H] \rangle$ | σ | $[X/H]_E$ | $[X/H]_L$ |
|-----|-----|-------------------------|---------------|-------------------------|----------|-----------|-----------|
| (1) | (2) | (3) | (4) | (5) | (6) | (7) | (8) |
| C | 4 | 8.55* | 8.56 | -0.01* | (0.46) | -0.11 | +0.11 |
| N | 2 | 7.79 | 8.05 | -0.26 | (0.01) | | |
| O | 4 | 8.70 | 8.93 | -0.23 | (0.16) | +0.32 | +0.07 |
| Mg | 3 | 7.63 | 7.58 | +0.05 | (0.20) | +0.02 | |
| Al | 1 | 5.96 | 6.47 | -0.51 | (0.00) | | |
| Si | 6 | 7.53 | 7.55 | -0.02 | (0.16) | +0.28 | +0.36 |
| S | 4 | 7.08 [†] | 7.21 | -0.13 [†] | (0.42) | | |
| Ca | 9 | 6.14 | 6.36 | -0.22 | (0.23) | -0.18 | -0.49 |
| Sc | 4 | 3.34 | 3.10 | +0.24 | (0.27) | +0.69 | -1.28 |
| Ti | 7 | 5.03 | 4.99 | +0.04 | (0.36) | -0.12 | +1.19 |
| Cr | 5 | 5.64 [‡] | 5.67 | -0.03 [‡] | (0.46) | -0.14 | +0.64 |
| Mn | 2 | 4.97 | 5.39 | -0.42 | (0.23) | -0.05 | +1.27 |
| Fe | 24 | 7.38 | 7.50 | -0.12 | (0.24) | -0.24 | +0.48 |
| Ni | 8 | 6.06 [‡] | 6.25 | -0.19 [‡] | (0.44) | -0.18 | +1.19 |
| Zn | 3 | 4.74 | 4.60 | +0.14 | (0.83) | | |
| Sr | 2 | 2.39 | 2.90 | -0.51 | (0.16) | -2.08 | |
| Ba | 3 | 2.30 | 2.13 | +0.17 | (0.21) | +0.21 | -0.62 |

(1) Element. (2) Number of regions. (3) Mean abundances averaged over N regions. (4) Reference solar abundances, which were taken from [Anders and Grevesse \(1989\)](#) except for Fe (see Sect. 5.1). (5) Differential abundances relative to the Sun defined as $\langle [X/H] \rangle \equiv \langle A_*^X \rangle - A_{\odot}^X$. (6) Standard deviation of the mean abundance. (7) $[X/H]$ results of [Erspamer and North \(2003\)](#). (8) $[X/H]$ results of [Luck \(2017\)](#).

*Reduced by 0.26 dex without 90509080 region data.

[†]Reduced by 0.22 dex without 86758705 region data.

[‡]Increased by 0.20 dex without 45404570 region data.

[‡]Decreased by 0.13 dex without 46604690 region data.

is slightly subsolar by ~ 0.2 dex. Let us examine how this consequence compares with the results reported in the past publications. Table 5 gives our $[X/H]$ values (column 5) in comparison with those of [Erspamer and North \(2003\)](#) (column 7) and [Luck \(2017\)](#) (column 8).

The results of [Erspamer and North \(2003\)](#) may be favorably compared with ours. Actually, the difference ($|\Delta[X/H]|$) is $\lesssim 0.3$ dex for most cases, except for O (0.55 dex), Sc (0.45 dex), Mn (0.37 dex), and Sr (1.57 dex). Therefore, although the discrepancy of Sr is extraordinarily large, their determinations are more or less tolerably consistent in view of the technical difference (e.g., their neglect of non-LTE effect) and inevitably lower precision of this kind of analysis.

In contrast, serious inconsistencies are observed regarding the results of [Luck \(2017\)](#). While the differences are several tenths dex

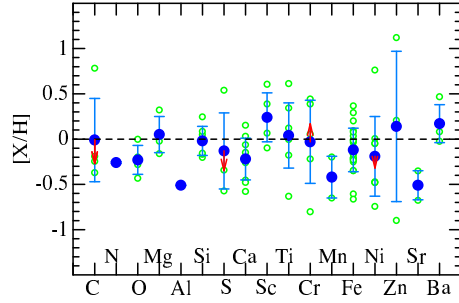


Fig. 6 The $[X/H]$ values (differential abundance of element X relative to the Sun) of 17 elements resulting from the analysis of this study. The mean values of $\langle [X/H] \rangle$ (averaged over available regions) are shown by blue bullets, where the error bars indicate the standard deviations. The individual $[X/H]$ results of each spectrum region are also depicted by green open circles. The red arrows (shown in the plots of C, S, Cr, and Ni) indicate the amount/direction of changes if the outlier data were excluded (see Sect. 5.7).

and not very conspicuous for lighter elements ($Z \leq 20$), intolerably large discrepancies amounting to $\lesssim 1-2$ dex are seen; e.g., Sc (1.52 dex), Ti (1.15 dex), Cr (0.67 dex), Mn (1.69 dex), Fe (0.60 dex), Ni (1.38 dex), and Ba (0.79 dex). We should recall that [Luck \(2017\)](#)'s study was originally devoted to abundance determinations of FGK-type stars and thus his analysis procedure (e.g., adopted lines) may not have been adequately adapted to A-type stars of higher T_{eff} . Accordingly, we would not have to take this large discordance seriously.

7 Summary and conclusion

Altair is a very rapidly-rotating A-type star, for which a number of researchers have investigated its physical parameters by way of direct interferometric observations (e.g., oblateness, rotation velocity, inclination angle, radius or T_{eff} at the pole/equator, gravitational darkening, etc.)

However, few spectroscopic studies on its photospheric chemical abundances have been conducted so far because of the considerable technical difficulty, which stems from the fact that spectral lines are widely broadened and blurred by rapid rotation and badly blended with each other. Moreover, the results of two available publications are apparently in conflict.

Motivated by this situation, we attempted a new spectroscopic analysis to establish the photospheric abundances of Altair while applying the

synthetic spectrum-fitting technique to its high-dispersion spectra. Our aim was to clarify whether or not this A-type star shows any chemical peculiarities (like Am stars or λ Boo stars).

The microturbulent velocity was determined by requiring that the dispersion of [M/H] (metallicity) vs. v_t relation (derived for 40 regions selected from violet–green wavelength ranges) be minimized, which yielded $v_t = 2.9 (\pm 0.9) \text{ km s}^{-1}$.

The abundances of 17 elements (C, N, O, Mg, Al, Si, S, Ca, Sc, Ti, Cr, Mn, Fe, Ni, Zn, Sr, Ba) were then derived from the spectrum-fitting analysis applied to 28 selected regions, where the non-LTE effect was taken into consideration for 12 elements (C, N, O, Mg, Al, Si, S, Ca, Sc, Ti, Zn, Sr, and Ba) while LTE was assumed for five Fe group elements (Ti, Cr, Mn, Fe, and Ni).

The resulting abundances tend to show considerable region-by-region dispersion (amounting to several tenths dex or even more), which reflects the difficulty of reliable abundance determination for very rapid rotator, though the following conclusions could be somehow extracted regarding the chemical characteristics of Altair.

First, the region-averaged differential abundances relative to the Sun are within $-0.5 \lesssim \langle [X/H] \rangle \lesssim +0.3$ for all elements, without showing any dependence upon Z (or any meaningful difference between volatile and refractory elements). Accordingly, we may rule out the possibility that Altair belongs to the group of chemically peculiar stars (such as Am stars or λ Boo stars).

Second, since [M/H] (mean metallicity derived as a by-product of v_t determination) ranges from ~ -0.2 to ~ -0.3 and the mean $\langle [X/H] \rangle$ averaged over all elements is between ~ -0.1 to ~ -0.2 , Altair’s metallicity is slightly subsolar (by ~ -0.2 dex on the average), which is likely to be attributed to chemical fluctuations in the primordial gas.

Acknowledgements. This research is based on the public-open data of the project “Spectroscopic Survey of Stars in the Solar Neighborhood” (Allende Prieto et al. 2004) as well as in part on those of the UVES Paranal Observatory Project (Bagnulo et al. 2003). This investigation has made use of the SIMBAD database, operated by CDS, Strasbourg, France, and the VALD database operated at Uppsala University, the Institute of

Astronomy RAS in Moscow, and the University of Vienna.

Supplementary information. The following online data are available as supplementary materials accompanied with this article.

- ReadMe.txt
- nltelines.dat
- reg_abund.dat

Declarations

- Funding
The author declares that no funds, grants, or other support were received during the preparation of this manuscript.
- Competing interests
The author has no relevant financial or non-financial interests to disclose.
- Author contributions
This investigation has been conducted solely by the author.

References

- Abt HA, Morrell NI (1995) The Relation between Rotational Velocities and Spectral Peculiarities among A-Type Stars. *Astrophys. J. Suppl. Ser.*99:135. <https://doi.org/10.1086/192182>
- Alekseeva GA, et al (1996) The Pulkovo Spectrophotometric Catalog of Bright Stars in the Range from 320 to 1080 NM. *Baltic Astron* 5:603. <https://doi.org/10.1515/astro-1996-0401>
- Allende Prieto C, Barklem PS, Lambert DL, et al (2004) S⁴N: A spectroscopic survey of stars in the solar neighborhood. The nearest 15 pc. *Astron. Astrophys.*420:183. <https://doi.org/10.1051/0004-6361:20035801>
- Anders E, Grevesse N (1989) Abundances of the elements: Meteoritic and solar. *Geochim Cosmochim Acta* 53:197. [https://doi.org/10.1016/0016-7037\(89\)90286-X](https://doi.org/10.1016/0016-7037(89)90286-X)
- Asplund M, Grevesse N, Sauval AJ, et al (2009) The Chemical Composition of the Sun. *Annu. Rev. Astron. Astrophys.*47:481. <https://doi.org/10.1146/annurev.astro.46.060407.145222>

- Bagnulo S, Jehin E, Ledoux C, et al (2003) The UVES Paranal Observatory Project: A Library of High-Resolution Spectra of Stars across the Hertzsprung-Russell Diagram. *Messenger* 114:10
- van Belle GT, Ciardi DR, Thompson RR, et al (2001) Altair's Oblateness and Rotation Velocity from Long-Baseline Interferometry. *Astrophys. J.*559:1155. <https://doi.org/10.1086/322340>
- Borisov SB, et al (2023) New Generation Stellar Spectral Libraries in the Optical and Near-infrared. I. The Recalibrated UVES-POP Library for Stellar Population Synthesis. *Astrophys. J. Suppl. Ser.*266:11. <https://doi.org/10.3847/1538-4365/acc321>
- Bouchaud K, Domiciano de Souza A, Rieutord M, et al (2020) A realistic two-dimensional model of Altair. *Astron. Astrophys.*633:A78. <https://doi.org/10.1051/0004-6361/201936830>
- Bouchet P, Manfroid J, Schmider FX (1991) JHKLM standard stars in the ESO system. *Astron. Astrophys. Suppl.*91:409
- Cohen M, Walker RG, Barlow MJ, et al (1992) Spectral Irradiance Calibration in the Infrared. I. Ground-Based and IRAS Broadband Calibrations. *Astron. J.*104:1650. <https://doi.org/10.1086/116349>
- Di Benedetto GP (1998) Towards a fundamental calibration of stellar parameters of A, F, G, K dwarfs and giants. *Astron. Astrophys.*339:858
- Ersparmer D, North P (2003) Automated spectroscopic abundances of A and F-type stars using echelle spectrographs. II. Abundances of 140 A-F stars from ELODIE. *Astron. Astrophys.*398:1121. <https://doi.org/10.1051/0004-6361:20021711>
- Gray RO, Corbally CJ, Garrison RF, et al (2003) Contributions to the Nearby Stars (NStars) Project: Spectroscopy of Stars Earlier than M0 within 40 Parsecs: The Northern Sample. I. *Astron. J.*126:2048. <https://doi.org/10.1086/378365>
- Hadjara M, et al (2014) Beyond the diffraction limit of optical/IR interferometers. II. Stellar parameters of rotating stars from differential phases. *Astron. Astrophys.*569:A45. <https://doi.org/10.1051/0004-6361/201424185>
- Kurucz RL (1993) ATLAS9 Stellar Atmosphere Programs and 2 km/s grid, Kurucz CD-ROM, No. 13. Harvard-Smithsonian Center for Astrophysics, Cambridge, MA
- Kurucz RL, Bell B (1995) Atomic Line Data, Kurucz CD-ROM, No. 23. Harvard-Smithsonian Center for Astrophysics, Cambridge, MA
- Lemke M (1993) Abundances in Rapidly Rotating A-Stars. In: Dworetzky MM, Castelli F, Faragiana R (eds) Peculiar versus Normal Phenomena in A-type and Related Stars, IAU Colloq. 138. Astronomical Society of the Pacific, San Francisco, CA, p 407
- Luck RE (2017) Abundances in the Local Region II: F, G, and K Dwarfs and Subgiants. *Astron. J.*153:21. <https://doi.org/10.3847/1538-3881/153/1/21>
- Mashonkina L, Ryabchikova T, Alexeeva S, et al (2020) Chemical diversity among A-B stars with low rotational velocities: non-LTE abundance analysis. *Mon. Not. R. Astron. Soc.*499:3706. <https://doi.org/10.1093/mnras/staa3099>
- Monnier JD, et al (2007) Imaging the Surface of Altair. *Science* 317:342. <https://doi.org/10.1126/science.1143205>
- Núñez PD, et al (2017) A near-infrared interferometric survey of debris-disc stars. VI. Extending the exozodiacal light survey with CHARA/JouFLU. *Astron. Astrophys.*608:A113
- Ohishi N, Nordgren TE, Hutter DJ (2004) Asymmetric Surface Brightness Distribution of Altair Observed with the Navy Prototype Optical Interferometer. *Astrophys. J.*612:463. <https://doi.org/10.1086/422422>
- Peterson DM, et al (2006) Resolving the Effects of Rotation in Altair with Long-Baseline Interferometry. *Astrophys. J.*636:1087. <https://doi.org/10.1086/5000000>

10.1086/497981

- Ryabchikova T, Piskunov N, Kurucz RL, et al (2015) A major upgrade of the VALD database. *Phys Scr* 90:054005. <https://doi.org/10.1088/0031-8949/90/5/054005>
- Sokolov NA (1995) The determination of Teff of B, A and F main sequence stars from the continuum between 3200Å and 3600Å. *Astron. Astrophys. Suppl.*110:553
- Domiciano de Souza A, Kervella P, Jankov S, et al (2005) Gravitational-darkening of Altair from interferometry. *Astron. Astrophys.*442:567. <https://doi.org/10.1051/0004-6361:20042476>
- Takeda Y (1991) Study on the non-LTE effect of Fe in stellar atmospheres: application to Arcturus. *Astron. Astrophys.*242:455
- Takeda Y (1992) Statistical Equilibrium and Abundances of Carbon and Nitrogen in the Atmosphere of Vega. *Publ. Astron. Soc. Jpn*44:649
- Takeda Y (1995) Self-Consistent Multi-Parameter Fitting of Stellar Flux Spectra. *Publ. Astron. Soc. Jpn*47:287. <https://doi.org/10.1093/pasj/47.3.287>
- Takeda Y (2003) Oxygen line formation in late-F through early-K disk/halo stars. infrared O I triplet and [O I] lines. *Astron. Astrophys.*402:343. <https://doi.org/10.1051/0004-6361:20030217>
- Takeda Y (2020) Behaviors of Ca II K line in A-type stars. *Stars and Galaxies* 3:1. <https://doi.org/10.32231/starsandgalaxies.3.0.1>
- Takeda Y (2022a) Center-Limb Variation of Solar Photospheric Microturbulence. *Sol. Phys.*297:4. <https://doi.org/10.1007/s11207-021-01931-0>
- Takeda Y (2022b) Photospheric silicon abundances of upper main-sequence stars derived from Si II 6347/6371 doublet lines. *Contrib Astron Obs Skalnaté Pleso* 52:5. <https://doi.org/10.31577/caosp.2022.52.1.5>
- Takeda Y (2023a) Does the A-type Metallic-Line Star IW Persei Have Non-Uniform Chemical Anomaly on the Surface? *Acta Astron.*73:35. <https://doi.org/10.32023/0001-5237/73.1.3>
- Takeda Y (2023b) Photospheric aluminium abundances of A-type main-sequence stars. *Contrib Astron Obs Skalnaté Pleso* 53:31. <https://doi.org/10.31577/caosp.2023.53.2.31>
- Takeda Y (2025) Spectroscopic Study of the Late B-type Eclipsing Binary System AR Aurigae A and B: Towards Clarifying the Differences in Atmospheric Parameters and Chemical Abundances. *Res Astron Astrophys* 25:025016. <https://doi.org/10.1088/1674-4527/adaa48>
- Takeda Y (2026) Barium Abundances of A–F–G Type Stars in the Hyades Cluster. *Astron Nachr* 347:e70060. <https://doi.org/10.1002/asna.70060>
- Takeda Y, Hashimoto O, Taguchi H, et al (2005) Non-LTE Line-Formation and Abundances of Sulfur and Zinc in F, G, and K Stars. *Publ. Astron. Soc. Jpn*57:751. <https://doi.org/10.1093/pasj/57.5.751>
- Takeda Y, Kawanomoto S, Ohishi N (2008) Rotational Feature of Vega Revealed from Spectral Line Profiles. *Astrophys. J.*678:446. <https://doi.org/10.1086/528949>
- Venn K, Lambert DL (1990) The Chemical Composition of Three Lambda Bootis Stars. *Astrophys. J.*363:234. <https://doi.org/10.1086/169334>
- Zorec J, Royer F (2012) Rotational velocities of A-type stars. IV. Evolution of rotational velocities. *Astron. Astrophys.*537:A120. <https://doi.org/10.1051/0004-6361/201117691>